

## HARNESSING THE ANTIOXIDANT PROPERTY OF CERIUM AND YTTRIUM OXIDE NANOPARTICLES TO ENHANCE MESENCHYMAL STEM CELL PROLIFERATION

HADEER A AGLAN<sup>1,2</sup>, MOSTAFA MABROUK<sup>3</sup>, RIHAM M ALY<sup>2,4</sup>, HANAN H BEHEREI<sup>3</sup>, HANAA H AHMED<sup>1,2\*</sup>

<sup>1</sup>Hormones Department, National Research Centre, Giza, Egypt. <sup>2</sup>Stem Cells Lab, Center of Excellence for Advanced Sciences, National Research Centre, Giza, Egypt. <sup>3</sup>Refractories, Ceramics and Building Materials Department, National Research Centre, Giza, Egypt. <sup>4</sup>Basic Dental Science Department, National Research Centre, Giza, Egypt. Email: hanaaomr@yahoo.com

Received: 23 January 2018, Revised and Accepted: 2 August 2018

### ABSTRACT

**Objective:** This work was designed to explore if cerium oxide (CeO<sub>2</sub>) and yttrium oxide (Y<sub>2</sub>O<sub>3</sub>) nanoparticles as antioxidant agents could potentiate the proliferation of mesenchymal stem cells (MSCs) derived from human dental pulp (hDPSCs).

**Methods:** Nanoparticles were characterized by transmission electron microscopy, particle size and zeta potential, X-ray diffraction, Fourier-transform infrared spectroscopy, and scanning electron microscope (SEM) along with energy-dispersive X-ray spectrometry. Furthermore, MSCs were isolated from human dental pulp, propagated and characterized by flow cytometry. Thereafter, the proliferative impact of the suggested nanoparticles on hDPSCs was investigated by 3-(4,5)-dimethylthiazol)-2,5-diphenyl tetrazolium bromide assay.

**Results:** Different sizes (14.09–26.50 nm and 18.80–31.31 nm) for CeO<sub>2</sub> and Y<sub>2</sub>O<sub>3</sub> respectively, morphology, charges, and proliferative efficacy in hDPSCs were recorded for both nanoparticles.

**Conclusion:** Generally speaking, the tested nanoparticles heightened the proliferative response of hDPSCs with the most prominent effect exerted by 15 µg/ml of CeO<sub>2</sub> and 5 µg/ml of Y<sub>2</sub>O<sub>3</sub>. It is reasonable to assume that the antioxidant property of CeO<sub>2</sub> and Y<sub>2</sub>O<sub>3</sub> be involved in strengthening the proliferation process of hDPSCs.

**Keywords:** Mesenchymal stem cells, Cerium oxide nanoparticles, Yttrium oxide nanoparticles, Antioxidant effect, Proliferative impact.

© 2018 The Authors. Published by Innovare Academic Sciences Pvt Ltd. This is an open access article under the CC BY license (<http://creativecommons.org/licenses/by/4.0/>) DOI: <http://dx.doi.org/10.22159/ajpcr.2018.v11i9.27914>

### INTRODUCTION

The particular target of tissue engineering is to promote the repairment of the destroyed tissue and maintain its functional features [1]. Clinical usage of dental stem cells as biological progenitor candidates for tissue regeneration was recently reported [2]. However, there are many factors hinder the clinical application of mesenchymal stem cells (MSCs) such as culturing obstacles, high transformation risk, and down proliferation rate *in vitro* [3]. Furthermore, many studies showed some drawbacks, because of lower viability of the transplanted cells. Particularly, about 99% of implanted cells died at the 1<sup>st</sup> h after the implantation process and this could be owed to the harshness of the human biological environment that the cells face on implantation [4,5]. One of the major causative factors for implanted cell death is oxygen deficiency due to delayed revascularization at the site of implantation [6].

Intracellular oxidative stress may be developed during the isolation of cells, multiple handling, and preparation steps of the sample as well as addition of proteolytic enzymes at reseeding stage. Earlier reports have mentioned that the increase in the intracellular reactive oxygen species (ROS) levels in the lag phase of cell growth is capable of suppressing the rate of proliferation [7]. Therefore, different approaches were intended to oppose the biological microenvironmental stress facing the cells before the transplantation procedures. Among these developed strategies is the *in vitro* introduction of nanoparticles rare earth oxides into MSCs cultures in order to be utilized as free radical quenchers within these cells [8].

Cerium oxide (CeO<sub>2</sub>) nanoparticles, also known as nanoceria, have a great potential to scavenge superoxide anions, hydrogen peroxide, and peroxynitrite *in vivo* [9]. Depending on the surface oxidation state, +3/+4, nanoceria could mimic the activity of the cellular antioxidant enzymes, superoxide dismutase and catalase [10,11]. Aside from these properties, CeO<sub>2</sub> nanoparticles could augment angiogenesis through

adjusting the intracellular oxygen environment and stabilizing hypoxia inducing factor 1 $\alpha$  endogenously [12].

Yttrium oxide (Y<sub>2</sub>O<sub>3</sub>), a vastly utilized host material for various rare earth dopants, is of interest for its potency to be applied in biological imaging and photodynamic therapy [13]. Y<sub>2</sub>O<sub>3</sub> has been shown to protect rat pancreatic islets from oxidative stress-mediated apoptosis [14]. Y<sub>2</sub>O<sub>3</sub> nanoparticles are well known as excellent free radical scavengers due to their non-stoichiometric crystal defects [15].

Although the therapeutic influence of CeO<sub>2</sub> and Y<sub>2</sub>O<sub>3</sub> nanoparticles was previously studied with different cell lines, their antioxidant and proliferative effects on the human dental pulp-derived mesenchymal stem cells (hDPSCs) *in vitro* have not been reported yet. The above motivations were investigated in a comparative manner between CeO<sub>2</sub> and Y<sub>2</sub>O<sub>3</sub> nanoparticles. It is relevant to note that different techniques such as transmission electron microscopy (TEM), particle size and zeta potential, X-ray diffraction (XRD), Fourier-transform infrared (FTIR), and scanning electron microscope (SEM) coupled with energy-dispersive X-ray spectrometry (EDX) were applied for the studied nanoparticles to demonstrate their size, morphology, potential charges, physicochemical characters, and elemental properties before conducting the *in vitro* assay.

### METHODS

#### Nanoparticles

Cerium (IV) oxide (CeO<sub>2</sub>) and yttrium (III) oxide (Y<sub>2</sub>O<sub>3</sub>) nanoparticles were purchased from Sigma-Aldrich (St Louis, Missouri, USA).

#### Size and morphology of the nanoparticles: Transmission electron microscopy (TEM)

TEM was used to analyze the crystal structure, size, and morphology of the investigated nanoparticles. Practically, TEM images were recorded

for CeO<sub>2</sub> and Y<sub>2</sub>O<sub>3</sub> nanoparticles using TEM, JEOL JEM-2100 with an accelerating voltage of 200 kV.

#### Size distribution and zeta potential: Dynamic light scattering (DLS) zetasizer

Electrophoretic measurements were obtained using a Zetasizer Nano ZS (Malvern Instruments, UK) equipped with a 633-nm laser. The reference standard (DTS1230, zeta-potential standard from Malvern) was used to qualify the performance of the instrument. Samples (50 mg) were suspended in 10 ml of deionized water and were filtered using a 0.22- $\mu$ m filter before analysis. Sample preparation involved filling of a disposable capillary cell (DTS1060, Malvern). Before their use, these cells were thoroughly cleaned with ethanol and deionized water, as recommended by the instrument vendor. For analysis, the individual cell was filled with the appropriate sample and flushed before refilling; measurement was carried out on the second filling. Malvern Instrument's Dispersion Technology software (Version 4.0) was used for data analysis, and zeta-potential values were estimated from the measured electrophoretic mobility data using the Smoluchowski equation.

#### Physicochemical characterizations: XRD

XRD patterns of CeO<sub>2</sub> and Y<sub>2</sub>O<sub>3</sub> nanoparticles were measured by using Rigaku X-ray diffractometer. The monochromatic X-rays with a wavelength of 0.1542 nm were generated using a Cu K $\alpha$  source with an emission current of 200 mA and a voltage of 40 kV. Samples scans were measured from 5 to 60° at a scan speed of 4°/min.

#### Physicochemical characterizations: FTIR analysis

FTIR analysis was used to investigate the functional groups of the CeO<sub>2</sub> and Y<sub>2</sub>O<sub>3</sub> nanoparticles. Before analysis, 2 mg of nanopowders were mixed with 200 mg KBr in the mortar and grinded into a fine powder then pressed into solid disks of 0.5 cm diameter. FTIR spectra were recorded using a Perkin Elmer Spectrum 2000 FTIR spectrometer, employing a single-reflection diamond MIRTGS detector (PerkinElmer Spectrum 100, Llantrisant, Wales, UK). All samples were analyzed by a universal FTIR spectrum series at a resolution of 4 cm<sup>-1</sup>.

#### Microstructure and elemental composition: SEM-EDX analysis

The morphology and the elemental analysis of CeO<sub>2</sub> and Y<sub>2</sub>O<sub>3</sub> nanoparticles were conducted using SEM with EDX. SEM images were recorded using a JEOL JXA-840A, Electronprobe microanalyzer, Japan, at 15 kv. Samples were rendered electrically conductive before analysis through gold-sputter coating (SPI Module™ Sputter Coater, SPI Supplies, PA) and were attached to the SEM stub using adhesive carbon tape.

#### Derivation and maintenance of hDPSCs

This study was approved by the Ethical Committee of the Medical Research of the National Research Centre, Egypt (Approval no.16386). hDPSCs were isolated from human dental pulp of adult subjects undergoing routine tooth extraction according to Gronthos *et al.* [16] protocol. The collected tissue was digested in solution of 0.2% Collagenase type II (Serva Electrophoresis GmbH). The isolated dental pulp cells cultured in fresh Dulbecco's modified Eagle's medium (DMEM, Lonza, Belgium) supplemented with 10% fetal bovine serum (FBS, Lonza) were incubated at 37°C and 5% CO<sub>2</sub>. Medium was changed twice per week thereafter. Once the cells became 80%–90% confluent, they were passaged. On the time of passaging, the cells in each culture dish were treated with 0.5% trypsin/EDTA (Lonza).

#### Cell surface antigen analysis

After the third passage, hDPSCs were released by trypsinization. The cells were incubated with FITC-conjugated CD 34 (Dako Co., Denmark) or PE-conjugated CD 90 (R and D Systems, UK) antibodies for 30 min at 4°C and PE-conjugated CD 105 (Miltenyi Biotec, Germany) antibody for 10 min at 4°C followed by flow cytometric analysis using Beckman Coulter Elite XL, USA instrument.

#### Proliferative assay

hDPSCs proliferation was determined using 3-[4,5-dimethylthiazol-2-yl]-2,5 diphenyl tetrazolium bromide (MTT, Sigma, USA) assay according to the method of van Meerloo *et al.* [17]. Briefly, hDPSCs were seeded in 96-well plates at the density of 1 × 10<sup>4</sup> cells/well and cultured for 12 h under 5% CO<sub>2</sub> and 37°C. Thereafter, each one of the suggested nanoparticles at various concentrations (2, 5, 10, 15, 20, and 25  $\mu$ g/ml) was added per well. Media without drug were added as control. After 24, 48, and 72 h incubations, MTT dissolved in PBS was added to each well at a final concentration of 5 mg/ml, and the samples were incubated at 37°C for 4 h. Water-insoluble crystals of formazan that formed during MTT cleavage in actively metabolizing cells were then dissolved in dimethyl sulfoxide. Absorbance was measured at 450 nm, using a microplate reader (Model 500; BIO-RAD Instrument Inc., USA). The cells proliferation (%) was calculated and compared with the control.

#### Statistical analyses

All experiments were carried out at least in triplicate, and data were expressed as mean  $\pm$  standard deviation.

## RESULTS AND DISCUSSION

#### Size and morphology of the nanoparticles

The transmission electron microscopic analysis was conducted to assert the actual size, morphology of the nanoparticles, their growth pattern, and the distribution of the crystallites. TEM analysis of CeO<sub>2</sub> nanoparticles showed uniform nanostructures of nanocubes with an average diameter of 18.80–31.31 nm and length of 84.17 nm (Fig. 1a). The obtained result matches to the CeO<sub>2</sub> nanoparticles early reported by Li *et al.* [18]. On the other side, the morphology of Y<sub>2</sub>O<sub>3</sub> nanoparticles demonstrated a high homogeneity of semispherical-shaped nanoparticles with a diameter in the range of 14.09–26.50 nm (Fig. 1b). This result comes in the line with the previous study of Soga *et al.* [19].

#### Size distribution and zeta potential of the nanoparticles

Size distribution and zeta potential are vital and very advantageous factors in the investigation of the nanoparticle properties and cell materials interaction. Fig. 2a represents the particle size of CeO<sub>2</sub> in the deionized water. An average particle size of CeO<sub>2</sub> was 469.4 nm in 100% as obtained from the DLS measurement which is considered a little bit higher as compared to the particle size shown in the TEM image of CeO<sub>2</sub>. The higher particle size (obtained from DLS measurement) could be owed to the expected agglomerations and the dynamic scattering of the nanoparticles within the dispersion medium [20]. The zeta potential of CeO<sub>2</sub> at the same conditions is illustrated in Fig. 2b as it is expressed by two peaks +2.53 and –137 mV with the area % values 77 and 23%, respectively.

The size distribution of Y<sub>2</sub>O<sub>3</sub> nanoparticles is measured at the above-mentioned conditions and depicted in Fig. 2c. It is noted that the Y<sub>2</sub>O<sub>3</sub> nanoparticles exhibited a smaller average particle size of 46.1 nm in 100% compared to that observed for CeO<sub>2</sub> nanoparticles as confirmed

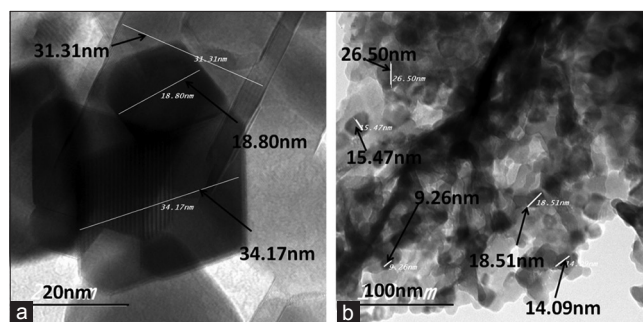


**Fig. 1: Transmission electron microscopy images of (a) cerium oxide and (b) yttrium oxide nanoparticles**

by the DLS measurement. This result is consistent with the TEM finding although, the obvious size difference between the two measurements owing to their different operating techniques. The zeta potential of  $Y_2O_3$  shown in Fig. 2d exhibited only one peak of  $Y_2O_3$  obtained at  $-0.442$  mV with the area percentage value of 100%.

#### XRD analysis of the nanoparticles

To speculate the physical phases and phase purity of the nanoparticles under investigation, XRD analysis was conducted.  $CeO_2$  nanoparticles elicited characteristic peaks, which are very close to the cubic phase of structured  $CeO_2$  crystal (Fig. 3a). The characteristic peaks corresponding to the (111), (200), (220), (311), (222), (400), (331), (420), and (422) planes are located at  $2\theta = 29.2^\circ, 33.1^\circ, 47.5^\circ, 57.6^\circ, 59.0^\circ, 64.5^\circ, 76.7^\circ, 79.2^\circ,$  and  $88.4^\circ$ , respectively. This result fits the recently reported finding of Farahmandjou *et al.* [21]. Moreover, no peaks of any other phase were registered indicating the high purity of the  $CeO_2$  nanoparticles. In addition, the sharp diffraction peaks that are observed for the  $CeO_2$  nanoparticles emphasize the small sizes of  $CeO_2$  crystallites as well as a homogeneous arrangement. These data echo those previously cited by Atta *et al.* [22].

The physical phase of the  $Y_2O_3$  nanoparticles was inspected by the XRD analysis, and the spectrum is shown in Fig. 3b. The obtained peaks are corresponded, respectively, to the (222), (400), (411), (332), (431), (440), (611), and (622) planes of main crystalline  $Y_2O_3$  nanoparticles

phase. These results are consistent with the Joint Committee on Powder Diffraction Standards, card No. 41-1105. The room temperature lattice parameter of the unit cell of the yttria phase estimated by the XRD pattern is matched with the JCPDS database of number 83-0927. Weak peaks for MgO at  $2\theta = 37.1, 43.4,$  and  $62.5^\circ$  are also detected (Fig. 3b).

#### FTIR spectra of the nanoparticles

FTIR measurements were conducted for the subjected nanoparticles to elucidate the chemical integrity of the particles, and the spectra are represented in Fig. 4. The  $CeO_2$  nanoparticle FTIR spectrum is shown in Fig. 4a, in the range of  $400-4000\text{ cm}^{-1}$  wave numbers. In details, the large broad band is observed at  $3415\text{ cm}^{-1}$  which is ascribed to the O-H stretching vibration in  $OH^-$  groups. Absorption band is noted around  $1464\text{ cm}^{-1}$  which is assigned to the bending vibration of  $CO_2$  stretching. The intense band at  $500\text{ cm}^{-1}$  corresponds to the Ce-O stretching vibration. The bands located at  $741, 750,$  and  $1036\text{ cm}^{-1}$  have been attributed to the  $CO_2$  asymmetric stretching vibration,  $CO_3^{2-}$  bending vibration, and C-O stretching vibration, respectively. The bands located at  $1298\text{ cm}^{-1}$  are attributed to carbonate species vibrations [23].

The FTIR spectrum for  $Y_2O_3$  is illustrated in Fig. 4b. Absorption bands are observed around  $500$  and  $600\text{ cm}^{-1}$ , corresponding to oxygen metal as reported for  $Y_2O_3$  by Jeong and Bae [24]. The bands noted around  $1640$  and  $1555\text{ cm}^{-1}$  correspond to asymmetric stretching of C-O band which may arise from the absorption of  $CO_2$  from the atmosphere.

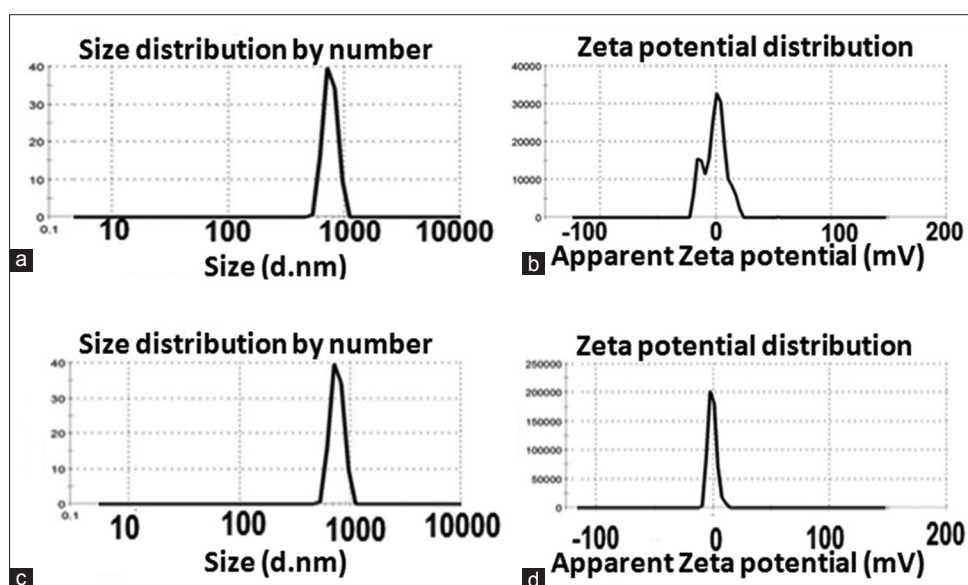


Fig. 2: Illustrates of (a) size distribution, (b) zeta potentials of cerium oxide nanoparticles, (c) size distribution, and (d) zeta potentials of yttrium oxide nanoparticles

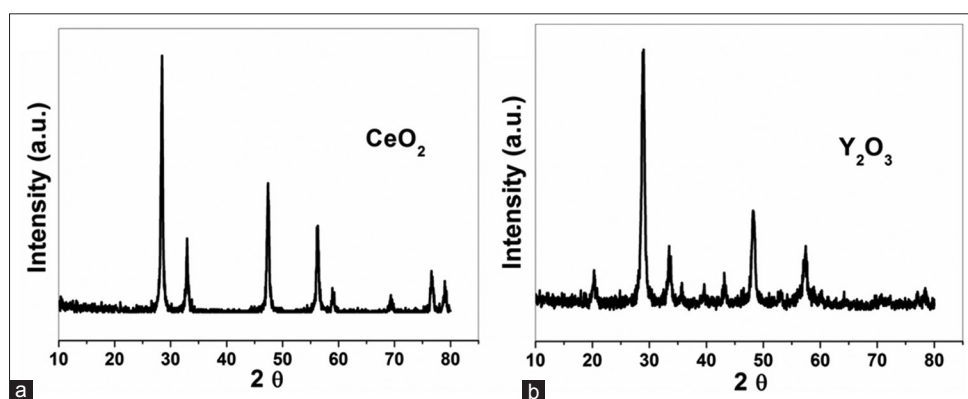


Fig. 3: X-ray diffraction of (a) cerium oxide and (b) yttrium oxide nanoparticles

The bands observed in the region of 3647.14–3403.46  $\text{cm}^{-1}$  and 1508.23  $\text{cm}^{-1}$  may be due to the presence of OH stretching and bending vibration modes, respectively. This phenomenon may be resulting from both hydroxyl groups and strongly adsorbed molecular water in the crystal lattice of yttrium hydroxide [24]. This is obviously noted in the frequency region of 3470–3200  $\text{cm}^{-1}$  for both oxides which may be attributed to vibrational mode of OH, resulting from the presence of moisture in KBr disc. The bands observed at 526.53–694.33  $\text{cm}^{-1}$  are assigned to the stretching vibration of Y–O bonds as mentioned in the previous study of Schwartz and Schwartz [25].

**SEM measurements and elemental analysis of the nanoparticles**

Undoubtedly, the purity and the morphology of the nanoparticles are very critical factors in studying the cells-nanomaterials interactions. Therefore, SEM measurements and elemental analysis of the two nanoparticles are conducted and showed in Fig. 5. In general, both nanoparticles exhibited similar morphology of fused and aggregated nanoparticles. The EDX of  $\text{CeO}_2$  nanoparticles is shown in Fig. 5a which confirmed its purity as only Ce and O elements are detected. The presence of very minor impurity (C and F) in  $\text{CeO}_2$  is also noted which may be adsorbed from the atmosphere or due to the sample handling. The EDX of  $\text{Y}_2\text{O}_3$  as shown in Fig. 5b documented its purity as only Y

and O elements are detected. The presence of very minor impurity (C and Al) in  $\text{Y}_2\text{O}_3$  is also observed which may be adsorbed from the atmosphere or due to the sample handling.

**MSC surface markers**

Flow cytometric analysis revealed that hDPSCs are positive for CD90 (98.5%) and CD105 (99.5%) and negative for CD34 (0.81%) as represented in Fig. 6. Similar results were previously reported for hDPSCs obtained from various cryopreservation methods of human dental pulp tissues of diseased teeth [26].

**Effect of nanomaterials on MSC proliferation**

Cell viability was quantitatively estimated employing colorimetric MTT assay that detects the mitochondrial activity of the cells. The MTT assay is based on the reduction of the yellow tetrazolium dye MTT to a purple water-insoluble formazan in cells bearing intact mitochondria and hence reflects the state of cultured cells. MTT assay results showed that the percentage viability of hDPSCs treated with  $\text{CeO}_2$  nanoparticles at concentrations of 15, 20, and 25  $\mu\text{g/ml}$  for 24 h are about 134.3, 124.4, and 117%, respectively (Fig. 7a), compared to the negative control (cells alone), while the percentage viability of hDPSCs treated with  $\text{CeO}_2$  nanoparticles at concentrations of 15, 20, and 25  $\mu\text{g/ml}$  for

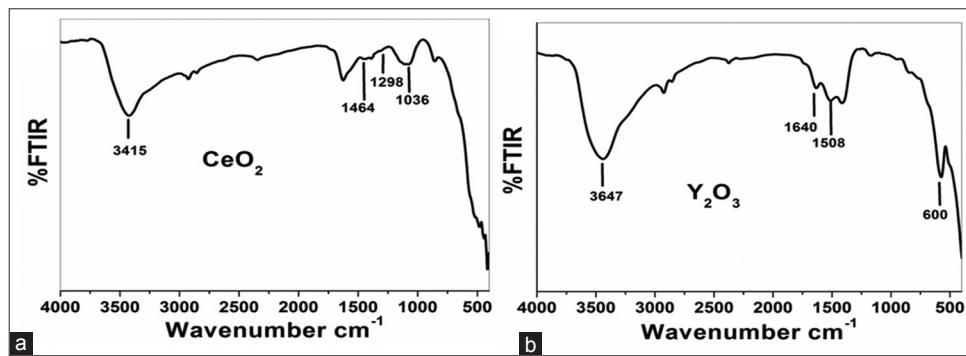


Fig. 4: Fourier-transform infrared spectroscopy of (a) cerium oxide and (b) yttrium oxide nanoparticles

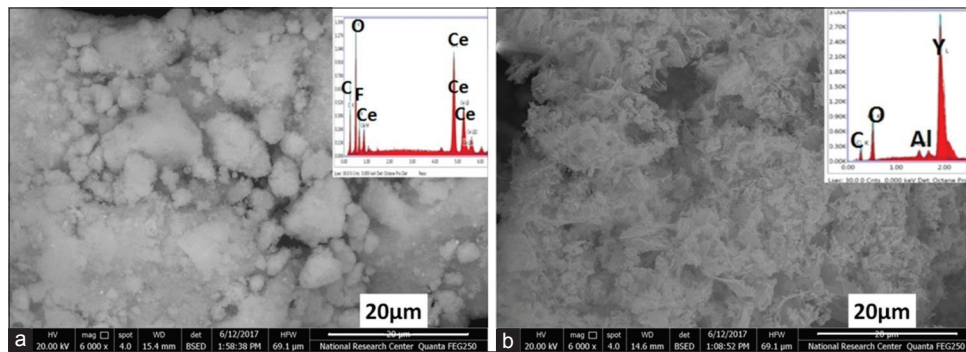


Fig. 5: Scanning electron microscope images and energy-dispersive X-ray spectrometry of (a) cerium oxide and (b) yttrium oxide nanoparticles

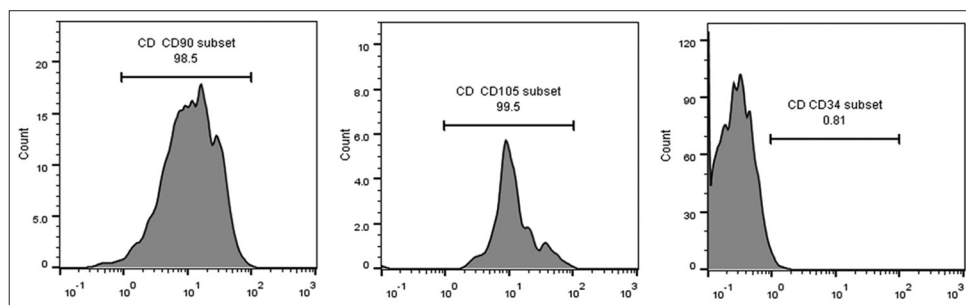
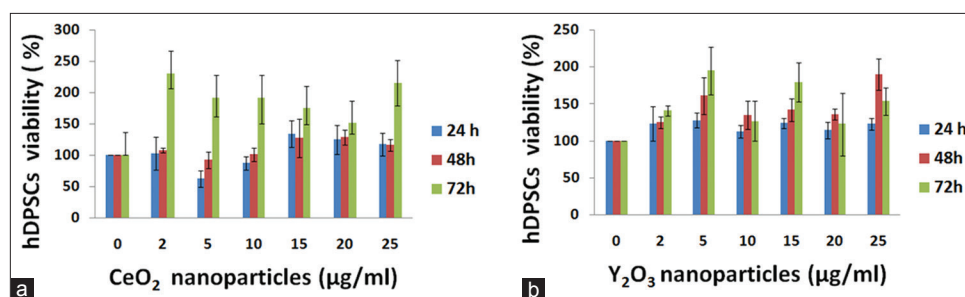


Fig. 6: Flow cytometric analysis of human dental pulp stem cells after staining with CD34, CD90, and CD105 antibodies



**Fig. 7: Proliferation and viability of human dental pulp stem cells in the presence of different concentrations of (a) cerium oxide and (b) yttrium oxide nanoparticles for 24, 48, and 72 h (results are mean±standard deviation of the triplicate experiments)**

48 h are about 127.2, 128.4, and 116%, respectively (Fig. 7a), compared to the negative control. After 72 h, treatment of hDPSCs with 2 and 25 µg/ml of CeO<sub>2</sub> nanoparticles experienced marked positive impact on their percentage viability (229.7 for 2 µg/ml and 215.1% for 25 µg/ml of CeO<sub>2</sub> nanoparticles) compared to the negative control (Fig. 7a). At the same time, the percentage viability of hDPSCs treated with CeO<sub>2</sub> nanoparticles at concentrations of 5, 10, 15, and 20 µg/ml for 72 h are about 190.9, 191.8, 174.4, and 150.7%, respectively (Fig. 7a), compared to the negative control.

The percentage viability of hDPSCs treated with Y<sub>2</sub>O<sub>3</sub> nanoparticles at concentrations of 2, 5, 15, and 25 µg/ml for 24 h are about 123.3, 127.6, 124, and 123%, respectively, compared to the negative control (Fig. 7b). After 48 h, treatment of hDPSCs with Y<sub>2</sub>O<sub>3</sub> nanoparticles at a concentration of 25 µg/ml evoked marked positive effect on cell percentage viability (190.1%) compared to the negative control (Fig. 7b). The percentage viability of hDPSCs treated with Y<sub>2</sub>O<sub>3</sub> nanoparticles at concentrations of 2, 5, 10, 15, and 20 µg/ml for 48 h are about 124.7, 160.5, 134.6, 142, and 135.8%, respectively, compared to the negative control (Fig. 7b). The percentage viability of hDPSCs treated with Y<sub>2</sub>O<sub>3</sub> nanoparticles at concentration of 5 µg/ml for 72 h is about 194.5% compared to the negative control (Fig. 7b). Furthermore, after 72 h, the percentage viability of hDPSCs treated with Y<sub>2</sub>O<sub>3</sub> nanoparticles at concentrations of 2, 10, 15, 20, and 25 µg/ml are about 140.6, 126.5, 179.5, 122.4, and 153.4%, respectively, compared to the negative control (Fig. 7b).

The remediation of biomedical materials, especially nanomaterials to MSCs, was found to be a promising tactic to modulate the cell functions particularly cell proliferation and differentiation into particular progenies [27-29]. Alteration of the antioxidant activity plays a key role in maintaining the optimum intracellular redox balance which is important for conserving the normal functioning of cellular systems, including DNA repair and stem cells signaling [30]. For stem cells, the intracellular redox balance is very critical, as the intracellular ROS level and genomic stability are related closely [31] and their imbalance resulted in spontaneous differentiation [32], loss of stemness [33], or transformation [34].

Based on our data, the chosen nanoparticles confer relatively different proliferative effect on hDPSCs. These findings go hand in hand with the previous reports carried out by Zhang *et al.* [35] who cited that CeO<sub>2</sub> nanoparticles enhance the viability of bone marrow-derived MSCs at all tested concentrations with evident dose dependence for 24 and 72 h. Popov *et al.* [36] mentioned that the introduction of nanocrystalline CeO<sub>2</sub> doped with gadolinium (Ce<sub>1-x</sub>Gd<sub>x</sub>O<sub>y</sub>) into dental MSC culture promotes the cells proliferation in a dose-dependent manner. Moreover, a study on normal human colon cells proved that CeO<sub>2</sub> nanoparticles rescued cell viability and reduced ROS production after irradiation [37]. Furthermore, CeO<sub>2</sub> nanoparticles were found to quench free radicals in murine insulinoma cells treated with hydroquinone and in cultured retinal neurons treated with H<sub>2</sub>O<sub>2</sub> [38]. Normal lung fibroblasts were protected from radiation-induced cell death by CeO<sub>2</sub> nanoparticles [39]. Likewise, Li *et al.* [40] mentioned that ternary biomaterial composed of nHA/PA66/yttria-stabilized tetragonal zirconia increases the

proliferation of osteoblast precursor cell line (MC3T3-E1 cells). Ghaznavi *et al.* [41] reported that both CeO<sub>2</sub> and Y<sub>2</sub>O<sub>3</sub> nanoparticles enhanced the survival of undifferentiated rat pheochromocytoma cells exposed to high glucose-induced oxidative stress.

Both CeO<sub>2</sub> and Y<sub>2</sub>O<sub>3</sub> nanoparticles are known as free radicals scavengers [41]. Mandoli *et al.* [42] suggested that the ability of CeO<sub>2</sub> nanoparticles to enhance the growth and promote the adhesion and proliferation of MSCs in a biodegradable polymer matrix could possibly ascribed to its antioxidant activity. Antioxidants are believed to decrease intracellular ROS levels [43], and intracellular ROS plays a key role in regulating cell adhesion and cell proliferation [44]. As the increased levels of intracellular ROS during the initial period of cell growth delay their transition from the resting stage and initiation of proliferation [7]. Furthermore, earlier studies documented that low levels of ROS can affect pluripotent stem cell proliferation through controlling various signaling pathways including mitogen-activated protein kinase, nuclear factor kappa-light-chain-enhancer of activated B cells, and Wnt axis [45,46]. Furthermore, Kim *et al.* [47] found that low levels of ROS potentiate the proliferation and migration of MSCs by regulating the extracellular signal-regulated kinase and Jun-1/2 pathways. It has been reported that CeO<sub>2</sub> nanoparticles can accelerate the proliferation of primary mouse embryonic fibroblasts through attenuating the intracellular ROS levels during the lag phase of cell growth and modifying the expression level of the major antioxidant enzymes [48]. Sun *et al.* [49] demonstrated that antioxidant treatment augments the entry of MSCs into the S phase by repressing cyclin-dependent kinase (CDK) inhibitors and results in rapid cell proliferation. They speculated that antioxidants can alter the cell cycle progression of MSCs by downregulating CDK and CDK4 inhibitors and upregulating CDK2, CDK4, and cell division cycle protein 2 homolog expression.

From another point of view, Horie *et al.* [50] cited that CeO<sub>2</sub> nanoparticles have the ability to adsorb Ca<sup>2+</sup>-ions from culture medium and, on entering the cell cytoplasm, activate calcium-dependent proteins and consequently affect intracellular signaling pathways and the overall cell metabolism.

It would be pertinent to mention that the nanomaterials experienced the optimal proliferative effect on hDPSCs in the current work are negatively charged as indicated from their zeta potential data. In fact, the nanoparticle infiltration within the hDPSCs is thought to be controlled by more than one parameter, including the particles size, morphology, and charge [51-53]. According to the TEM and DLS measurements, the Y<sub>2</sub>O<sub>3</sub> nanoparticles recorded less particle size (14.09–26.50 nm) than the CeO<sub>2</sub> nanoparticles (18.80–31.31 nm). On the other side, the cell proliferation results demonstrated lower cell viability for the Y<sub>2</sub>O<sub>3</sub> nanoparticles compared to that of CeO<sub>2</sub> nanoparticles. Furthermore, negative charge (–137 mV) with higher value was recorded for CeO<sub>2</sub> nanoparticles compared with positive charge with little tendency to negativity recorded for the Y<sub>2</sub>O<sub>3</sub> nanoparticles (0.442 mV) as evidenced by DLS measurements. All the results suggested that the selected nanoparticles-cells interactions are highly dependent on the nanoparticles charge. This emphasizes the impressive role of nanoparticles charges over the particle size (limited to the nanoscale).

## CONCLUSION

The morphology, size, and charge of the chosen rare earth oxide nanoparticles were successfully investigated in a comparatively manner using specified tools. The present scenario gave us a valuable insight in the interpretation of the nanoparticles/cells interaction to come out with an acceptable idea about their mechanism of action as antioxidant agents. The potentiality of the chosen nanoparticles in improving the proliferation rate of MSCs seems to be linked with their ability to quench free radicals and maintain the optimal intracellular redox balance.

## ACKNOWLEDGMENT

This work was financially supported by the National Research Centre (Egypt) under Grant no: 11010134.

## AUTHOR'S CONTRIBUTION

Hadeer A. Aglan: Responsible for determining the proliferative effect of suggested nanoparticles on hDPSCs and writing and revising the manuscript. Mostafa Mabrouk: Responsible for physicochemical characterization of the chosen nanoparticles, interpretation of data, and writing and revising the manuscript; Riham M. Aly: Responsible for isolating and propagating hDPSCs and revising the manuscript; Hanan H. Beherei: Responsible for physicochemical characterization of the chosen nanoparticles, interpretation of data, and revising the manuscript; and Hanaa H. Ahmed: Responsible for study concept, interpretation of data, and writing and revising the manuscript.

## CONFLICTS OF INTEREST

The authors declare that they have no conflicts of interest.

## REFERENCES

- Murray PE, Garcia-Godoy F, Hargreaves KM. Regenerative endodontics: A review of current status and a call for action. *J Endod* 2007;33:377-90.
- Chen FM, Gao LN, Tian BM, Zhang XY, Zhang YJ, Dong GY, et al. Treatment of periodontal intrabony defects using autologous periodontal ligament stem cells: A randomized clinical trial. *Stem Cell Res Ther* 2016;7:33.
- Zhang F, Ren T, Wu J, Niu J. Small concentrations of TGF- $\beta$  1 promote proliferation of bone marrow-derived mesenchymal stem cells via activation of Wnt/ $\beta$ -Catenin pathway. *Indian J Exp Biol* 2015;53:508-13.
- Copland IB, Galipeau J. Death and inflammation following somatic cell transplantation. *Semin Immunopathol* 2011;33:535-50.
- Trounson A, McDonald C. Stem cell therapies in clinical trials: Progress and challenges. *Cell Stem Cell* 2015;17:11-22.
- Rouwkema J, Koopman B, Blitterswijk C, Dhert W, Malda J. Supply of nutrients to cells in engineered tissues. *Biotechnol Genet Eng Rev* 2010;26:163-78.
- Muller F, Lustgarten M, Jang Y, Richardson A, Van Remmen H. Trends in oxidative aging theories. *Free Radic Biol Med* 2007;43:477-503.
- Guin R, Banu S, Kurian GA. Synthesis of copper oxide nanoparticles using *Desmodium gangeticum* aqueous root extract. *Int J Pharm Pharm Sci* 2015;7:60-5.
- Arya A, Gangwar A, Singh SK, Roy M, Das M, Sethy NK, et al. Cerium oxide nanoparticles promote neurogenesis and abrogate hypoxia-induced memory impairment through AMPK-PKC-CBP signaling cascade. *Int J Nanomed* 2016;23:1159-73.
- Heckert EG, Karakoti AS, Seal S, Self WT. The role of cerium redox state in the SOD mimetic activity of nanoceria. *Biomaterials* 2008;29:2705-9.
- Pirmohamed T, Dowding JM, Singh S, Wasserman B, Heckert E, Karakoti AS, et al. Nanoceria exhibit redox state-dependent catalase mimetic activity. *Chem Commun (Camb)* 2010;46:2736-8.
- Das S, Singh S, Dowding JM, Oommen S, Kumar A, Sayle TX, et al. The induction of angiogenesis by cerium oxide nanoparticles through the modulation of oxygen in intracellular environments. *Biomaterials* 2012;33:7746-55.
- Chang ML, Tie SL. Fabrication of novel luminor Y2O3: Eu3+@ SiO2 @ YVO4: Eu3+ with core/shell hetero nanostructure. *Nanotechnology* 2008;19:75711.
- Hosseini A, Baeeri M, Rahimifard M, Navaei-Nigjeh M, Mohammadirad A, Pourkhalili N, et al. Antiapoptotic effects of cerium oxide and yttrium oxide nanoparticles in isolated rat pancreatic islets. *Hum Exp Toxicol* 2013;32:544-53.
- Mitra RN, Merwin MJ, Han Z, Conley SM, Al-Ubaidi MR, Naash MI. Yttrium oxide nanoparticles prevent photoreceptor death in a light-damage model of retinal degeneration. *Free Radic Biol Med* 2014;75:140-8.
- Gronthos S, Brahim J, Li W, Fisher LW, Cherman N, Boyde A, et al. Stem cell properties of human dental pulp stem cells. *J Dent Res* 2002;81:531-5.
- van Meerloo J, Kaspers GJ, Cloos J. Cell sensitivity assays: The MTT assay. *Methods Mol Biol* 2011;731:237-45.
- Li J, Zhang Z, Gao W, Zhang S, Ma Y, Qu Y. Pressure regulations on the surface properties of CeO<sub>2</sub> nanorods and their catalytic activity for CO-oxidation and nitrile hydrolysis reactions. *ACS Appl Mater Interfaces* 2016;8:22988-96.
- Soga K, Okumura Y, Tsuji K, Venkatachalam N. Effect of K3PO4 addition as sintering inhibitor during calcination of Y2O3 nanoparticle. *J Phys* 2009;191:1-7.
- Mahapatra C, Singh RK, Lee JH, Jung J, Hyun JK, Kim HW. Nano-shape varied cerium oxide nanomaterials rescue human dental stem cells from oxidative insult through intracellular or extracellular actions. *Acta Biomater* 2017;50:142-53.
- Farahmandjou M, Zarinkamar M, Firoozabadi TP. Synthesis of cerium oxide (CeO<sub>2</sub>) nanoparticles using simple CO-precipitation method. *Rev Mex Fisic* 2016;62:496-9.
- Atta AH, El-Shenawy AI, Koura FA, Refat MS. Synthesis and characterization of some selenium nanometric compounds: Spectroscopic, biological and antioxidant assessments. *World J Nano Sci Eng* 2014;4:58-69.
- Phoka S, Laokul P, Swatsitang E, Promarak V, Seraphin S, Maensiri S. Synthesis, structural and optical properties of CeO<sub>2</sub> nanoparticles synthesized by a simple polyvinyl pyrrolidone (PVP) solution route. *Mater Chem Phys* 2009;115:423-8.
- Jeong KJ, Bae DS. Synthesis and characterization of Y2O3 powders by a modified solvothermal process. *Korean J Mater Res* 2012;22:78-81.
- Schwartz CA, Schwartz J. Surface modification of Y2O3 nanoparticles. *Langmuir* 2007;23:9158-916.
- Chen YK, Huang AH, Chan AW, Shieh TY, Lin LM. Human dental pulp stem cells derived from different cryopreservation methods of human dental pulp tissues of diseased teeth. *J Oral Pathol Med* 2011;40:793-800.
- Lutolf MP, Gilbert PM, Blau HM. Designing materials to direct stem-cell fate. *Nature* 2009;462:433-41.
- Powar PV. Development status in the meadow of nanostructure magnetic drug delivery system and its promising applications. *Int J Pharm Pharm Sci* 2017;9:10-7.
- Davison MJ, McMurray RJ, Smith CA, Dalby MJ, Meek RD. Nanopit-induced osteoprogenitor cell differentiation: The effect of nanopit depth. *J Tissue Eng* 2016;7:2041731416652778.
- Valle-Prieto A, Conget PA. Human mesenchymal stem cells efficiently manage oxidative stress. *Stem Cells Dev* 2010;19:1885-93.
- Li TS, Marb'an E. Physiological levels of reactive oxygen species are required to maintain genomic stability in stem cells. *Stem Cells* 2010;28:1178-85.
- Higuchi M, Dusting GJ, Peshavariya H, Jiang F, Hsiao ST, Chan EC, et al. Differentiation of human adipose-derived stem cells into fat involves reactive oxygen species and forkhead box o1 mediated upregulation of antioxidant enzymes. *Stem Cells Dev* 2013;22:878-88.
- Perales-Clemente E, Folmes CD, Terzic A. Metabolic regulation of redox status in stem cells. *Antioxid Redox Signal* 2014;21:1648-59.
- Mathieu J, Zhou W, Xing Y, Sperber H, Ferreccio A, Agoston Z, et al. Hypoxia-inducible factors have distinct and stage specific roles during reprogramming of human cells to pluripotency. *Cell Stem Cell* 2014;14:592-605.
- Zhang Q, Ge K, Ren H, Zhang C, Zhang J. Effects of cerium oxide nanoparticles on the proliferation, osteogenic differentiation and adipogenic differentiation of primary mouse bone marrow stromal cells *in vitro*. *J Nanosci Nanotechnol* 2015;15:6444-51.
- Popov AL, Tatarnikova OG, Popova NR, Selezneva II, Akkizov AY, Ermakov AM, et al. Ce1-xGdxOy nanoparticles stimulate proliferation of dental pulp stem cells *in vitro*. *Nano Hybrids Composites* 2017;13:26-31.
- Colon J, Hsieh N, Ferguson A, Kupelian P, Seal S, Jenkins DW, et al. Cerium oxide nanoparticles protect gastrointestinal epithelium from radiation-induced damage by reduction of reactive oxygen

- species and upregulation of superoxide dismutase 2. *Nanomedicine* 2010;6:698-705.
38. Tsai YY, Oca-Cossio J, Agering K, Simpson NE, Atkinson MA, Wasserfall CH, *et al.* Novel synthesis of cerium oxide nanoparticles for free radical scavenging. *Nanomedicine (Lond)* 2007;2:325.
  39. Colon J, Herrera L, Smith J, Patil S, Komanski C, Kupelian P, *et al.* Protection from radiation-induced pneumonitis using cerium oxide nanoparticles. *Nanomedicine* 2009;5:225.
  40. Li Y, Li H, Zhang J, Zhao W, Shen J, Jiang D. *In vitro* evaluation of an yttria-stabilized zirconia reinforced nano-hydroxyapatite/polyamide 66 ternary biomaterial: Biomechanics, biocompatibility and bioactivity. *RSC Adv* 2016;6:114086-95.
  41. Ghaznavi H, Najafi R, Mehrzadi S, Hosseini A, Tekyemarroof N, Shakeri-zadeh A, *et al.* Neuro-protective effects of cerium and yttrium oxide nanoparticles on high glucose-induced oxidative stress and apoptosis in undifferentiated PC12 cells. *Neurol Res* 2015;37:624-32.
  42. Mandoli C, Pagliari F, Pagliari S, Forte G, Di Nardo P, Licocchia S, *et al.* Stem cell aligned growth induced by CeO<sub>2</sub> nanoparticles in PLGA scaffolds with improved bioactivity for regenerative medicine. *Adv Funct Mater* 2010;20:1617.
  43. Kanda Y, Hinata T, Kang SW, Watanabe Y. Reactive oxygen species mediate adipocyte differentiation in mesenchymal stem cells. *Life Sci* 2011;89:250-8.
  44. Song H, Cha MJ, Song BW, Kim IK, Chang W, Lim S, *et al.* Reactive oxygen species inhibit adhesion of mesenchymal stem cells implanted into ischemic myocardium via interference of focal adhesion complex. *Stem Cells* 2010;28:555-63.
  45. Jeong AY, Lee MY, Lee SH, Park JH, Han HJ. PPARdelta agonist-mediated ROS stimulates mouse embryonic stem cell proliferation through cooperation of p38 MAPK and wnt/beta-catenin. *Cell Cycle* 2009;8:611-9.
  46. Lee SH, Lee YJ, Han HJ. Effect of arachidonic acid on hypoxia-induced IL-6 production in mouse ES cells: Involvement of MAPKs, NF-kappaB, and HIF-1alpha. *J Cell Physiol* 2010;222:574-85.
  47. Kim J, Song S, Park S, Song S, Xia Y, Sung J. Primary involvement of NADPH oxidase 4 in hypoxia induced generation of reactive oxygen species in adipose derived stem cells. *Stem Cells Dev* 2012;21:2212-21.
  48. Popov AL, Popova NR, Selezneva II, Akkizov AY, Ivanov VK. Cerium oxide nanoparticles stimulate proliferation of primary mouse embryonic fibroblasts *in vitro*. *Mat Sci Eng C* 2016;68:406-13.
  49. Sun LY, Pang CY, Li DK, Liao CH, Huang WC, Wu CC, *et al.* Antioxidants cause rapid expansion of human adipose-derived mesenchymal stem cells via CDK and CDK inhibitor regulation. *J Biomed Sci* 2013;20:53.
  50. Horie M, Nishio K, Kato H, Fujita K, Endoh S, Nakamura A, *et al.* Cellular responses induced by cerium oxide nanoparticles: Induction of intracellular calcium level and oxidative stress on culture cells. *J Biochem* 2011;150:461-71.
  51. Gratton SE, Ropp PA, Pohlhaus PD, Luft JC, Madden VJ, Napier ME, *et al.* The effect of particle design on cellular internalization pathways. *Proc Natl Acad Sci U S A* 2008;105:11613-8.
  52. Agarwal R, Roy K. Intracellular delivery of polymeric nanocarriers: A matter of size, shape, charge, elasticity and surface composition. *Ther Deliv* 2013;4:705-23.
  53. Agarwal R, Singh V, Jurney P, Shi L, Sreenivasan SV, Roy K. Mammalian cells preferentially internalize hydrogel nanodiscs over nanorods and use shape specific uptake mechanisms. *Proc Natl Acad Sci U S A* 2013;110:17247-52.